Journal of
Materials Chemistry C

Materials for optical, magnetic and electronic devices

Accepted Manuscript

This article can be cited before page numbers have been issued, to do this please use: F. Q. Huang, Y. Fang, Q. Dong, J. Pan, H. Liu, P. Liu, Q. Li, Y. Sun, W. Zhao and B. Liu, *J. Mater. Chem. C*, 2019, DOI: 10.1039/C9TC02417D.

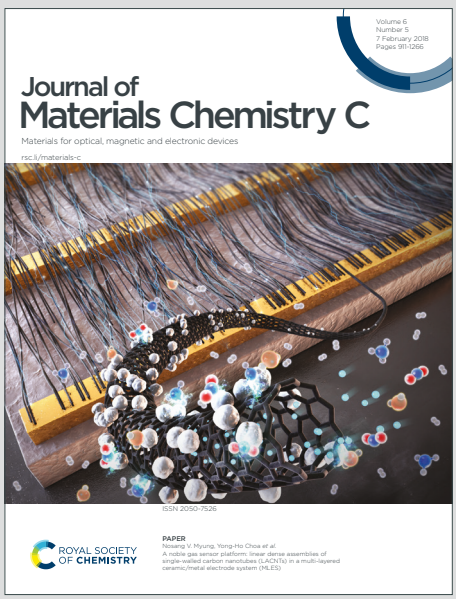

ROYAL SOCIETY OF CHEMISTRY

rsc.li/materials-c

View Article Online
DOI: 10.1039/C9TC02417D

COMMUNICATION

Observation of Superconductivity in Pressurized 2M WSe_2 Crystals

Yuqiang Fang,†[ab] Qing Dong,†[f] Jie Pan,†[e] Hanyu Liu,[f] Pan Liu,[d] Yiyang Sun,[a] Quanjun Li,[f] Wei Zhao,*[a] Bingbing Liu*[f] and Fuqiang Huang*[ac]

Received 00th January 20xx,
Accepted 00th January 20xx

DOI: 10.1039/x0xx00000x

In this communication, we reported a new-phase 2M WSe_2 with a monoclinic space group C2/m. 2M WSe_2 presents a metallic behavior under ambient pressure and shows superconducting transition with a maximum T_c of 7.3 K at 10.7 GPa, which arises from the enhanced density of states near Fermi surface upon pressurization.

Transition metal dichalcogenides (TMDs) constructed by the distorted octahedrally coordinated 1T'- MX_2 monolayers (M = Mo, W; X = S, Se, Te) have attracted intensive attention due to their intriguing physiochemical properties such as superconductivity,[1-4] quantum spin Hall effect,[5-10] large magnetoresistance[11-12] and excellent electrocatalytic performance.[13-16] The physical properties of TMDs depend on the d-orbital electronic configurations of transition metal atoms to a great extent. Compared with semiconducting 2H phases, the 1T'-phase VIB-group TMDs are semimetallic due to the partially occupied d orbits. Recently, there are increasing reports about the superconductivity in 1T' phases. For example, exfoliated 1T'-MoS_2 nanosheets has a superconducting transition temperature of 4.6 K.[17] The 2M WS_2 shows a T_c of 8.8 K with calculated topological surface states.[18] In addition, superconductivity was induced in T_d WTe_2 by chemical intercalation, electrostatic gating and the proximity effect.[19-21]

High pressure is also an effective tool to tune the electronic properties of materials and further generate superconductivity. The TMDs are suitable for high-pressure research, because the layered structure with weak Van der Waals force can be changed a lot under the high pressure.[22-24] For instance, superconductivity emerges in semiconducting 2H MoS_2 under ultrahigh pressure of 220 GPa.[25] For the type-II Weyl semimetal T_d WTe_2, superconductivity emerges from the suppression of large magnetoresistance.[26] Except for sulfides and tellurides, the structural evolution and physical properties of 1T' selenides under pressure have not been reported due to absence of phase-pure crystals. Recently a direct solution-phase method synthesized the 1T' WSe_2 nanosheets.[27] The size and purity of the 1T' WSe_2 nanosheets are still unsuitable for the crystal structure determination and electrical transport measurements.

Here, we successfully obtained millimeter-sized 1T' WSe_2 single crystals by a topochemical reaction. The crystal structure of 1T' WSe_2 was determined by single crystal X-ray diffraction. According to the nomenclature of TMDs, 1T' WSe_2 should be called as 2M WSe_2 precisely because it has a monoclinic group and two WSe_2 layers in the unit cell. The electrical transport properties of 2M WSe_2 under high pressure was performed and superconductivity was observed in the resistance curves. Superconducting transition occurs at 4.2 GPa, and T_c increases to a maximum of 7.3 K at 10.7 GPa in the dome-shaped T-P phase diagram. Structural evolution of 2M WSe_2 was detected through the measurements of high-pressure synchrotron XRD. No structural transition happens in the superconducting regime. Moreover, electronic band structure calculations reveal that the density of states at Fermi surface increase rapidly upon pressurization, which could ac-count for the appearance and enhancement of T_c.

Since the metastable 2M WSe_2 crystals cannot be synthesized directly from high-temperature solid state reactions, we firstly synthesized the K_xWSe_2 crystals as precursor from the reaction of the K and 2H WSe_2 at 800 ^{0}C. Then, the K_xWSe_2 crystals were soaked in an oxidizing solution to extract K^+ ions to obtain 2M WSe_2 crystals, as depicted in the text of Supporting Information

[a] State Key Laboratory of High Performance Ceramics and Superfine Microstructure Shanghai Institute of Ceramics, Chinese Academy of Sciences, Shanghai, 200050, P. R. China. E-mail: huangfq@mail.sic.ac.cn
[b] University of Chinese Academy of Sciences, Beijing 100049, China
[c] State Key Laboratory of Rare Earth Materials Chemistry and Applications, College of Chemistry and Molecular Engineering, Peking University, Beijing 100871, China
[d] State Key Laboratory of Metal Matrix Composites, School of Materials Science and Engineering, Shanghai Jiao Tong University, Shanghai 200030, P. R. China
[e] Department of Materials Science and Engineering, City University of Hong Kong
[f] State Key Laboratory of Superhard Materials, Jilin University, Changchun 120012, China
† Y. Fang, Q. Dong and J, Pan contributed equally to this work.
Electronic Supplementary Information (ESI) available: [details of any supplementary information available should be included here]. See DOI: 10.1039/x0xx00000x

(SI). The crystal structure and refinement information of 2M WSe_2 are shown in **Table S1-S4**.

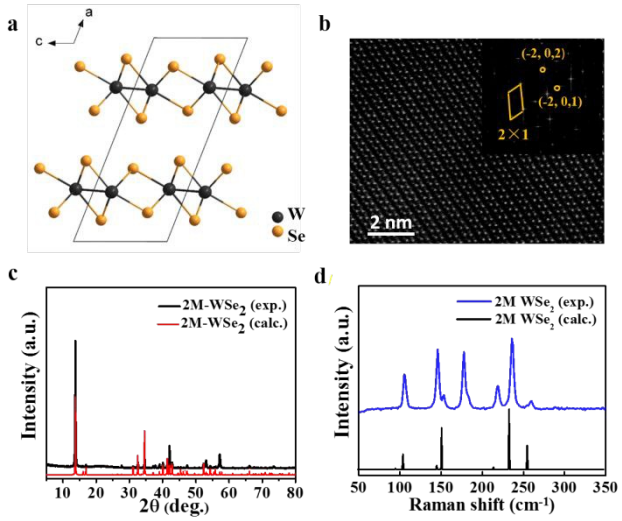

Figure 1. (a) The schematic structure of 2M WSe_2 from *b* axis. (b) High-resolution HADDF-STEM image of 2M WSe_2. Inset: the FFT of Figure b, which shows a × 2a superstructure clearly. (c) Powder X-ray diffraction pattern of the sample, where the red curve was theoretically calculated from the structure of 2M WSe_2. (d) Experimental and calculated Raman spectra of 2M WSe_2.

Figure 1a displays the schematic structure of 2M WSe_2, which crystallizes in a monoclinic space group of *C*2/m, with the lattice parameters, $a = 13.838(3)$Å, $b = 3.291(7)$Å, $c = 5.912(2)$Å and $\beta = 111.468(8)^0$. The unit cell of 2M WSe_2 consists of one independent W site and two independent Se sites. The W atom in 2M WSe_2 is coordinated to six Se atoms in a distorted octahedron, which buckles the Se atom layers. The coordination number of W atoms in 2M WSe_2 is eight due to the formation of W-W bonds.

The neighboring W atoms form linked zigzag chains with an equal bond length of 2.803(9) Å along the *b* axis. Besides, the W-Se bond lengths are equal to 2.600(1)Å, 2.630(2)Å 2.511(2)Å, and 2.536(2)Å respectively, compared with 2.526(1)Å in 2H WSe_2. The crystal structure of 2M WSe_2 is different from the known T_d WTe_2 owing to a different stacking pattern of 1T' MX_2 monolayers. The adjacent layers in T_d WTe_2 were rotated by 180° along the c axis, while the Se-W-Se sandwiched layers stack through transition along the *a* axis to build up 2M WSe_2 crystals.

The prepared 2M WSe_2 crystals are ribbon-shaped with hundreds of micrometers in length due to the preferred growth direction along the zigzag chains (along the *b* axis), as shown in scanning electron microscopy (SEM) image (**Figure S1**). The atomic structure of 2M WSe_2 was characterized by the high-angle annular dark-field scanning transmission electron microscopy (HAADF-STEM). **Figure 1b** shows the W-W zigzag chains clearly, which conforms to the schematic structure of 2M WSe_2. The Fourier transform (FFT) pattern (see the inset of **Figure 1b**) indicates a 1 × 2a superstructure. The PXRD pattern of the sample is shown in **Figure 1c**, where all the diffraction peaks fit well with the simulated diffraction data of 2M WSe_2. **Figure 1d** displays experimental and calculated Raman spectra of 2M WSe_2. Different from 2H WSe_2, there are seven peaks located at 106 cm^{-1}, 146 cm^{-1}, 154 cm^{-1}, 177 cm^{-1}, 218 cm^{-1}, 236 cm^{-1} and 259 cm^{-1} in the Raman spectrum, which match well with the calculated data.

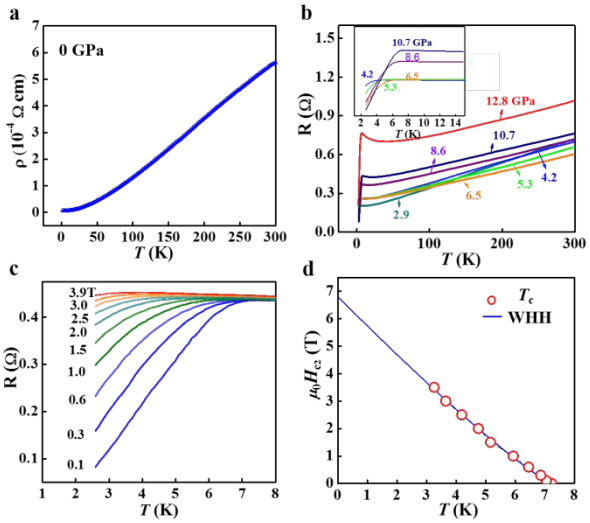

Figure 2. (a) The resistivity of 2M WSe_2 measured at ambient pressure. (b) Temperature dependence of electrical resistance measured at the pressures from 0.8 to 12.8 GPa. (c) The superconductivity transition of the 2M WSe_2 crystals at 10.7 GPa under the magnetic fields of up to 3.9 T. (d) Temperature dependence of the upper critical field for 2M WSe_2. The blue line represents fitting by the WHH formula.

The electrical transport properties of 2M WSe_2 were measured using normal four-point method on a single-crystal sample as shown in **Figure S2**. **Figure 2a** presents the temperature dependence of resistivity for 2M WSe_2 at ambient pressure. The resistivity decreases from 0.59 mΩ cm at 300 K to 6.18 μΩ cm at 2 K, suggesting a metallic behavior. No sign of superconducting transition is observed down to 2 K. Subsequently we investigated the electrical behavior of 2M WSe_2 under the quasi-hydrostatic pressure. **Figure 2b** shows temperature dependence of the resistance at the pressures from 2.9 GPa to 12.8 GPa. From the inset of **Figure 2b**, the superconducting sign of a slight drop in the resistance curves emerges at the pressure of 4.2 GPa with a critical temperature T_c of 4.3 K. Here T_c is defined as the temperature at which the resistance starts to deviate from the normal state. With increasing pressure, T_c shifts to higher temperature, and reaches a maximum of 7.3 K at 10.7 GPa. Zero resistance cannot been observed in all the resistance curves, which results from that the pressure gradients of the pressurized 2M WSe2 broaden the superconducting transition.[27] Above 10.7 GPa, superconductivity vanishes gradually. The pressure-temperature (P-T) phase diagram of 2M WSe_2 in **Figure S3** shows a dome-shaped superconductivity behavior, similar to that of T_d WTe_2 and 1T $TiSe_2$.[29-30]

To further confirm that the resistance drop in **Figure 2a** is superconducting transition, external magnetic field was applied perpendicular to the plane of 2M WSe_2 single crystal. **Figure 2c** shows the temperature dependence of the resistance under various magnetic fields at 10.7 GPa. The superconducting

transition was gradually suppressed with increasing field and a magnetic field of 4T almost smear out the superconductivity. This provides an important evidence of the presence of superconductivity in the pressurized 2M WSe_2 crystals. Furthermore, the superconductivity of 2M WSe2 can also be demonstrated by the measurements of magnetic susceptibility under high pressure (see the **Figure S3**). **Figure 2d** shows the critical temperature T_c dependence of the upper critical field $\mu_0 H_{c2}$, which can be fitted by the one-band Werthamer-Helfand-Hohenberg (WHH) formula $H_{c2}(T) = H_{c2}^*(1 - T/T_c)^{1+\alpha}$.[31] The zero-temperature $H_{c2}(0)$ is roughly estimated to be 6.79 T. In addition, the estimated value of $H_{c2}(0)$ is lower than the Pauli paramagnetic limit of $\mu_0 H_p = 1.84\ T_c = 13.4$ T for $T_c = 7.3$ K, which suggests no Pauli pair breaking. The nearly linear temperature dependence of H_{c2} may arise from an unconventional superconducting state or a multi-band Fermi surface topology. Usually, such linear temperature dependence of H_{c2} has also occurred in pressurized topological insulators Bi_2Se_3, pressurized Dirac semimetal Cd_3As_2 and unconventional superconductor YPtBi.[32-33]

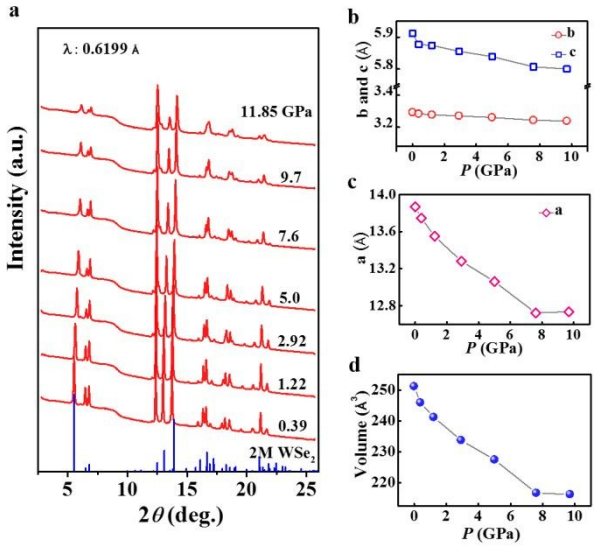

Figure 3. Structural information of 2M WSe_2 at high pressure. (a) XRD patterns of 2M WSe_2 collected at different pressure (λ= 0.6199 Å). (b-c) Pressure dependence of crystal lattice constants. (d) Pressure-dependent volume of unit cell.

The structural evolution of 2M WSe_2 crystals upon pressurization was measured through high-pressure synchrotron XRD (HPXRD) measurements at room temperature. **Figure 3a** shows the XRD patterns collected under the pressures from 0.39 to 11.85 GPa. The peaks move to higher angles with increasing pressure, which corresponds to the decrease of lattice parameters. Meanwhile, no extra peaks appeared, illustrating structure phase transition did not happen in this pressure regime. The lattice constants *a*, *b* and *c* dependence of pressure was shown in **Figure 3b-c**. The value of *a, b* and c decreases from 13.9 Å to 12.7 Å, 3.3 Å to 3.25 Å and 5.95 Å to 5.8 Å, respectively. The out-of-plane lattice can be compressed to a larger extent than the in-plane lattice due to the weak interlayer van der Waals interaction and strong intralayer chemical bonding. Moreover, it is interesting that the crystal can be compressed more hardly in the direction of *b* axis than *c* axis due to the existence of W-W metal bonding along *b* axis. **Figure S4** shows the phonon calculation calculated at 13.4 GPa. It can be seen that the phonon spectrum and DOS do not show any imaginary modes, suggesting that under this pressure the 2M structure can be kinetically stable. Combining the HPXRD data and calculated phonon spectrum, the superconductivity in the pressurized 2M WSe_2 does not arise from the structure transition.

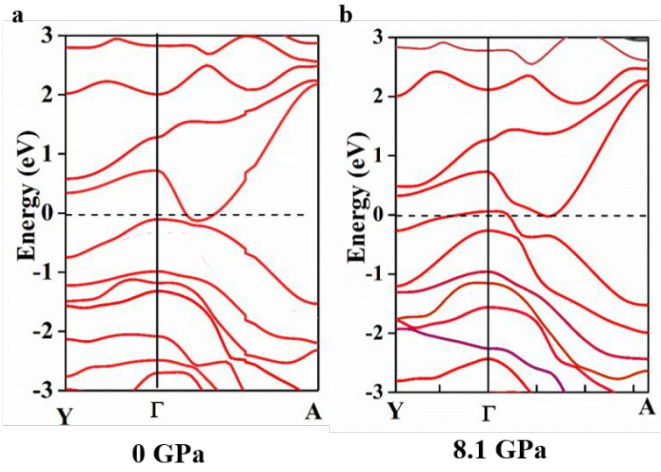

Figure 4. (a-b) The electronic band structure of 2M WSe_2 at pressures of 0 GPa and 8.1 GPa respectively.

The pressure-dependent electronic band structure of 2M WSe_2 has been calculated using density-function theory (DFT) calculations to understand the emergency of superconductivity in WSe_2 under high pressure. **Figure 4a-b** show the band structure at ambient pressure and 8.1 GPa respectively. The applied pressures can tune the electronic conditions near the Fermi surfaces. Compared to band structure at 0 GPa, there is a nearly flat band crossing the Fermi level at 8.1 GPa that enlarges the amount of carriers. It is this flat band that is responsible for the large DOS value at high pressure. **Figure S5** shows the calculated density of states at the Fermi surface under different pressures. DOS increases to a maximum and decreases gradually with increasing pressure, which is similar to the tendency of the observed T_c. For the T_d WTe_2, the adjacent Te-W-Te layers happen to slide upon compression resulting in a phase transition from T_d to 1T'. The structural transition leads to the emergency of superconductivity.[34] Although Se-W-Se layers in 2M WSe_2 do not slide below 11.85 GPa, the interlayer distance is closer and the interaction of Se 4*p* orbitals is enhanced, which can affect the band structure. Since no structure transition happens as entering the superconductivity states in high pressure, we suppose that the emergence and improvement of superconductivity in 2M WSe_2 results from enhanced DOS near Fermi surface under high pressure.

Conclusions

In summary, we successfully prepared 2M WSe_2 crystals and observed superconductivity in the pressurized sample. The T-P phase diagram exhibits a dome-shaped superconducting behavior that shows a maximum T_c of 7.3 K. Different from T_d WTe_2, no structural transition occur in the superconductivity region, confirmed by the high pressure XRD. According to the DFT calculations, N (E_F) at Fermi surface is enhanced with increasing pressure, accounting for the emergence of superconductivity and enhancement of T_c. Our work provides a new platform for the investigation of superconductivity in topological 1T'-phase TMDs.

Conflicts of interest

There are no conflicts to declare.

Acknowledgements

This work was financially supported by National key research and development program (Grant 2016YFB0901600), "Strategic Priority Research Program (B)" of the Chinese Academy of Sciences (Grant XDB04040200), Science and Technology Commission of Shanghai (Grant 16JC1401700), National Science Foundation of China (Grant 51672301), CAS Center for Excellence in Superconducting Electronics.

Notes and references

1 V. Fatemi, S. Wu, Y. Cao, L. Bretheau, Q. D. Gibson, K. Watanabe, T. Taniguchi, R. J. Cava, P. Jarillo-Herrero, *Science* **2018**, *362*, 926-929.
2 E. Sajadi, T. Palomaki, Z. Fei, W. Zhao, P. Bement, C. Olsen, S. Luescher, X. Xu, J. A. Folk, D. H. Cobden, *Science* **2018**, *362*, 922-926.
3 C. Shang, Y. Q. Fang, Q. Zhang, N. Z. Wang, Y. F. Wang, Z. Liu, B. Lei, F. B. Meng, L. K. Ma, T. Wu, Z. F. Wang, C. G. Zeng, F. Q. Huang, Z. Sun, X. H. Chen, *Phys. Rev. B* **2018**, *98,* 184513.
4 Y. Fang, J. Pan, J. He, R. Luo, D. Wang, X. Ce, K. Bu, W. Zhao, P. Liu, G. Mu, H. Zhang, T. Lin, F. Huang, *Ange. Chem.Int. Ed.* **2018**, *57*, 1232-1235.
5 X. Qian, J. Liu, L. Fu, J. Li, *Science* **2014**, *346*, 1344-1347.
6 F. Zheng, C. Cai, S. Ge, X. Zhang, X. Liu, H. Lu, Y. Zhang, J. Qiu, T. Taniguchi, K. Watanabe, S. Jia, J. Qi, J.-H. Chen, D. Sun, J. Feng, *Adv. Mater.***2016**, *28*, 4845-4851.
7 H. Xiang, B. Xu, J. Liu, Y. Xia, H. Lu, J. Yin, Z. Liu, *Aip Adv* **2016**, *6,*095005;
8 P. Chen, W. W. Pai, Y. H. Chan, W. L. Sun, C. Z. Xu, D. S. Lin, M. Y. Chou, A. V. Fedorov, T. C. Chiang, *Nat. Commun.* **2018**, *9, 2003*.
9 Y.-H. Song, Z.-Y. Jia, D. Zhang, X.-Y. Zhu, Z.-Q. Shi, H. Wang, L. Zhu, Q.-Q. Yuan, H. Zhang, D.-Y. Xing, S.-C. Li, *Nat. Commun.* **2018**, *9,* 4071.
10 S. Tang, C. Zhang, D. Wong, Z. Pedramrazi, H.-Z. Tsai, C. Jia, B. Moritz, M. Claassen, H. Ryu, S. Kahn, J. Jiang, H. Yan, M. Hashimoto, D. Lu, R. G. Moore, C.-C. Hwang, C. Hwang, Z. Hussain, Y. Chen, M. M. Ugeda, Z. Liu, X. Xie, T. P. Devereaux, M. F. Crommie, S.-K. Mo, Z.-X. Shen, *Nat. Phys.* **2017**, *13*, 683-689.
11 M. N. Ali, J. Xiong, S. Flynn, J. Tao, Q. D. Gibson, L. M. Schoop, T. Liang, N. Haldolaarachchige, M. Hirschberger, N. P. Ong, R. J. Cava, *Nature* **2014**, *514*, 205-210;
12 J. Jiang, F. Tang, X. C. Pan, H. M. Liu, X. H. Niu, Y. X. Wang, D. F. Xu, H. F. Yang, B. P. Xie, F. Q. Song, P. Dudin, T. K. Kim, M. Hoesch, P. K. Das, I. Vobornik, X. G. Wan, D. L. Feng, *Phys. Rev. Lett.* **2015**, *115*.
13 J. Ekspong, R. Sandstrom, L. P. Rajukumar, M. Terrones, T. Wagberg, E. Gracia-Espino, *Adv. Funct. Mater.* **2018**, *28,*1802744.
14 M. A. Lukowski, A. S. Daniel, C. R. English, F. Meng, A. Forticaux, R. J. Hamers, S. Jin, *Energy . Envir. Science* **2014**, *7*, 2608-2613.
15 I. H. Kwak, I. S. Kwon, H. G. Abbas, J. Seo, G. Jung, Y. Lee, D. Kim, J.-P. Ahn, J. Park, H. S. Kang, *J. Mater. Chem. A* **2019**, *7*, 2334-2343.
16 L. Liu, J. Wu, L. Wu, M. Ye, X. Liu, Q. Wang, S. Hou, P. Lu, L. Sun, J. Zheng, L. Xing, L. Gu, X. Jiang, L. Xie, L. Jiao, *Nat. Mater.* **2018**, *17*, 1108-1113.
17 C. Guo, J. Pan, H. Li, T. Lin, P. Liu, C. Song, D. Wang, G. Mu, X. Lai, H. Zhang, W. Zhou, M. Chen, F. Huang, *J Mater Chem C* **2017**, *5*, 10855-10860.
18 J. P. Yuqiang Fang, Dongqin Zhang, Dong Wang, Wei Zhao, Q. X. , Gang Mu, Haijun Zhang, Fuqiang Huang, *arXiv:* **2018**, *1808. 05324*.
19 C. Huang, A. Narayan, E. Zhang, Y. Liu, X. Yan, J. Wang, C. Zhang, W. Wang, T. Zhou, C. Yi, S. Liu, J. Ling, H. Zhang, R. Liu, R. Sankar, F. Chou, Y. Wang, Y. Shi, K. T. Law, S. Sanvito, P. Zhou, Z. Han, F. Xiu, *Acs Nano* **2018**, *12*, 7185-7196;
20 Q. Li, C. He, Y. Wang, E. Liu, M. Wang, Y. Wang, J. Zeng, Z. Ma, T. Cao, C. Yi, N. Wang, K. Watanabe, T. Taniguchi, L. Shao, Y. Shi, X. Chen, S.-J. Liang, Q.-H. Wang, F. Miao, *Nano. Lette.* **2018**, *18*, 7962-7968.
21 L. Zhu, Q.-Y. Li, Y.-Y. Lv, S. Li, X.-Y. Zhu, Z.-Y. Jia, Y. B. Chen, J. Wen, S.-C. Li, *Nano. Lette* **2018**, *18*, 6585-6590.
22 B. Liu, Y. Han, C. Gao, Y. Ma, G. Peng, B. Wu, C. Liu, Y. Wang, T. Hu, X. Cui, W. Ren, Y. Li, N. Su, H. Liu, G. Zou, *J.Phys. Chem. C* **2010**, *114*, 14251-14254.
23 A. P. Nayak, S. Bhattacharyya, J. Zhu, J. Liu, X. Wu, T. Pandey, C. Jin, A. K. Singh, D. Akinwande, J.-F. Lin, *Nat. Commun.* **2014**, *5,*3731;
24 Z.-H. Chi, X.-M. Zhao, H. Zhang, A. F. Goncharov, S. S. Lobanov, T. Kagayama, M. Sakata, X.-J. Chen, *Phys. Rev. Lett.* **2014**, *113,* 036802.
25 Z. Chi, X. Chen, F. Yen, F. Peng, Y. Zhou, J. Zhu, Y. Zhang, X. Liu, C. Lin, S. Chu, Y. Li, J. Zhao, T. Kagayama, Y. Ma, Z. Yang, *Phys. Rev. Lett.* **2018**, *120*.
26 D. Kang, Y. Zhou, W. Yi, C. Yang, J. Guo, Y. Shi, S. Zhang, Z. Wang, C. Zhang, S. Jiang, A. Li, K. Yang, Q. Wu, G. Zhang, L. Sun, Z. Zhao, *Nat. Commun.* **2015**, *6,* 7804.
27 Chi, Z.; Chen, X.; Yen, F.; Peng, F.; Zhou, Y.; Zhu, J.; Zhang, Y.; Liu, X.; Lin, C.; Chu, S.; Li, Y.; Zhao, J.; Kagayama, T.; Ma, Y.; Yang, Z. Superconductivity in Pristine 2H(a)-MoS2 at Ultrahigh Pressure, *Phys. Rev. Lett*. **2018**, 120, 037002.
28 M. S. Sokolikova, P. C. Sherrell, P. Palczynski, V. L. Bemmer, C. Mattevi, *Nat. Commun.* **2019**, *10,*712.
29 A. F. Kusmartseva, B. Sipos, H. Berger, L. Forro, E. Tutis, *Phys. Rev. Lett.* **2009**, *103,*236401.
30 X.-C. Pan, X. Chen, H. Liu, Y. Feng, Z. Wei, Y. Zhou, Z. Chi, L. Pi, F. Yen, F. Song, X. Wan, Z. Yang, B. Wang, G. Wang, Y. Zhang, *Nat. Commun.* **2015**, *6,*7805.
31 J. A. Woollam, R. B. Somoano, P. Oconnor, *Phys. Rev Lett.* **1974**, *32*, 712-714.
32 K. Kirshenbaum, P. S. Syers, A. P. Hope, N. P. Butch, J. R. Jeffries,

View Article Online
DOI: 10.1039/C9TC02417D

S. T. Weir, J. J. Hamlin, M. B. Maple, Y. K. Vohra, J. Paglione, *Phys. Rev. Lett.* **2013**, *111*, 087001.
33 T. V. Bay, T. Naka, Y. K. Huang, A. de Visser, *Phys. Rev. B* **2012**, *86,* 064515.
34 Zhou, Y.; Chen, X.; Li, N.; Zhang, R.; Wang, X.; An, C.; Zhou, Y.; Pan, X.; Song, F.; Wang, B.; Yang, W.; Yang, Z.; Zhang, Y. Pressure-induced Td to 1T ' structural phase transition in WTe_2. *Aip Adv* **2016**, *6*, 075008.